Approaching the Nucleon-Nucleon short-range repulsive core via the ^{4}He$(e, e'pN)$ triple-coincidence reaction.

I. Korover,[1] N. Muangma,[2] O. Hen,[1] R. Shneor,[1] V. Sulkosky,[2,3] A. Kelleher,[2] S. Gilad,[2] D. Higinbotham,[4] E. Piasetzky,[1] J. Watson,[5] S. Wood,[4] Abdurahim Rakhman,[6] P. Aguilera,[7] Z. Ahmed,[6] H. Albataineh,[8] K. Allada,[9] B. Anderson,[5] D. Anez,[10] K. Aniol,[11] J. Annand,[12] W. Armstrong,[13] J. Arrington,[14] T. Averett,[15] T. Badman,[15] H. Baghdasaryan,[16] X. Bai,[17] A. Beck,[18] S. Beck,[18] V. Bellini,[19] F. Benmokhtar,[20] W. Bertozzi,[2] J. Bittner,[3] W. Boeglin,[21] A. Camsonne,[4] C. Chen,[22] J. Chen,[4] K. Chirapatpimol,[16] E. Cisbani,[23] M. Dalton,[16] A. Daniel,[24] D. Day,[16] C.W. de Jager,[4,16] R. De Leo,[25] W. Deconinck,[2] M. Defurne,[26] D. Flay,[13] N. Fomin,[27] M. Friend,[20] S. Frullani,[23] E. Fuchey,[13] F. Garibaldi,[23] D. Gaskell,[4] R. Gilman,[28,4] O. Glamazdin,[29] C. Gu,[30] P. Gueye,[22] D. Hamilton,[12] C. Hanretty,[31] O. Hansen,[4] M. Hashemi Shabestari,[16] T. Holmstrom,[3] M. Huang,[32] S. Iqbal,[11] G. Jin,[16] N. Kalantarians,[33] H. Kang,[34] M. Khandaker,[4] J. LeRose,[4] J. Leckey,[35] R. Lindgren,[16] E. Long,[36] J. Mammei,[37] D. J. Margaziotis,[11] P. Markowitz,[21] A. Marti Jimenez-Arguello,[38] D. Meekins,[4] Z. Meziani,[13] R. Michaels,[4] M. Mihovilovic,[39] P. Monaghan,[2,22] C. Munoz Camacho,[38] B. Norum,[16] Nuruzzaman,[40] K. Pan,[2] S. Phillips,[36] I. Pomerantz,[1,41] M. Posik,[13] V. Punjabi,[42] X. Qian,[32] Y. Qiang,[32] X. Qiu,[43] P.E. Reimer,[14] S. Riordan,[16,44] G. Ron,[45] O. Rondon-Aramayo,[4] A. Saha,[4,*] E. Schulte,[28] L. Selvy,[5] A. Shahinyan,[46] S. Sirca,[47] J. Sjoegren,[12] K. Slifer,[36] P. Solvignon,[4] N. Sparveris,[13] R. Subedi,[16] W. Tireman,[48] D. Wang,[16] L. B. Weinstein,[8] B. Wojtsekhowski,[4] W. Yan,[49] I. Yaron,[1] Z. Ye,[16] X. Zhan,[2] J. Zhang,[4] Y. Zhang,[28] B. Zhao,[15] Z. Zhao,[16] X. Zheng,[16] P. Zhu,[49] and R. Zielinski[36]

(JLab Hall A E07006 Collaboration)

[1]*Tel Aviv University, Tel Aviv 69978, Israel*
[2]*Massachusetts Institute of Technology, Cambridge, MA 02139*
[3]*Longwood University, Farmville, VA 23909*
[4]*Thomas Jefferson National Accelerator Facility, Newport News, Virginia 23606*
[5]*Kent State University, Kent, OH 44242*
[6]*Syracuse University, Syracuse, NY 13244*
[7]*Institut de Physique Nucléaire (UMR 8608), CNRS/IN2P3 - Université Paris-Sud, F-91406 Orsay Cedex, France*
[8]*Old Dominion University, Norfolk, VA 23529*
[9]*University of Kentucky, Lexington, KY 40506*
[10]*Saint Mary's University, Halifax, Nova Scotia, Canada*
[11]*California State University, Los Angeles, Los Angeles, CA 90032*
[12]*University of Glasgow, Glasgow G12 8QQ, Scotland, United Kingdom*
[13]*Temple University, Philadelphia, PA 19122*
[14]*Physics Division, Argonne National Laboratory, Argonne, IL 60439*
[15]*College of William and Mary, Williamsburg, VA 23187*
[16]*University of Virginia, Charlottesville, VA 22904*
[17]*China Institute of Atomic Energy,Beijing, China*
[18]*Nuclear Research Center Negev, Beer-Sheva, Israel*
[19]*Universita di Catania, Catania, Italy*
[20]*Carnegie Mellon University, Pittsburgh, PA 15213*
[21]*Florida International University, Miami, FL 33199*
[22]*Hampton University, Hampton, VA 23668*
[23]*INFN, Sezione Sanità and Istituto Superiore di Sanità, 00161 Rome, Italy*
[24]*Ohio University, Athens, OH 45701*
[25]*INFN, Sezione di Bari and University of Bari, I-70126 Bari, Italy*
[26]*CEA Saclay, F-91191 Gif-sur-Yvette, France*
[27]*University of Tennessee, Knoxville, TN*
[28]*Rutgers, The State University of New Jersey, Piscataway, NJ 08855*
[29]*Kharkov Institute of Physics and Technology, Kharkov 61108, Ukraine*
[30]*Los Alamos National Laboratory, Los Alamos, NM 87545*
[31]*Florida State University, Tallahassee, FL 32306*
[32]*Duke University, Durham, NC 27708*
[33]*Unversity of Texas, Houston, TX 77030*
[34]*Seoul National University, Seoul, Korea*
[35]*Indiana University, Bloomington, IN 47405*
[36]*University of New Hampshire, Durham, NH 03824*
[37]*Virginia Polytechnic Inst. and State Univ., Blacksburg, VA*
[38]*Université Blaise Pascal/IN2P3, F-63177 Aubière, France*
[39]*Jozef Stefan Institute, Ljubljana, Slovenia*

[40]Mississippi State University, Miss. State, MS
[41]The University of Texas at Austin, Austin, Texas 78712
[42]Norfolk State University, VA 23504
[43]Lanzhou University, Lanzhou, China
[44]University of Massachusetts, Amherst, MA, 01006, USA
[45]Racah Institute of Physics Hebrew University of Jerusalem, Israel
[46]Yerevan Physics Institute, Yerevan 375036, Armenia
[47]Univ. of Ljubljana, Ljubljana, Slovenia
[48]Northern Michigan University
[49]University of Science and Technology, Hefei, China
(Dated: January 20, 2014)

We measured simultaneously the ^{4}He$(e,e'p)$, ^{4}He$(e,e'pp)$, and ^{4}He$(e,e'pn)$ reactions at $Q^2 = 2$ (GeV/c)^2 and $x_B > 1$, for a $(e,e'p)$ missing-momentum range of 400 to 830 MeV/c. The knocked-out proton was detected in coincidence with a proton or neutron recoiling almost back to back to the missing momentum, leaving the residual $A = 2$ system at low excitation energy. These data were used to identify two-nucleon short-range correlated pairs and to deduce their isospin structure as a function of missing momentum in a region where the nucleon-nucleon force is expected to change from predominantly tensor to repulsive. Neutron-proton pairs dominate the high-momentum tail of the nucleon momentum distributions, but their abundance is reduced as the nucleon momentum increases beyond ~ 500 MeV/c. The extracted fraction of proton-proton pairs is small and almost independent of the missing momentum in the range we studied. Our data are compared with *ab-initio* calculations of two-nucleon momentum distributions in ^{4}He.

The existence of stable nuclei is due to a delicate interplay between the long-range attraction that binds nucleons, and the short-range repulsion that prevents the collapse of the system. In between, the dominant scalar part of the nucleon-nucleon force almost vanishes and the interaction is dominated by the tensor force, which depends on the spin orientations and the relative orbital angular momentum of the nucleons.

Recent high-momentum-transfer triple-coincidence ^{12}C$(e,e'pN)$ and ^{12}C$(p,2pn)$ measurements [1–4] have shown that nucleons in the nuclear ground state form pairs with large relative momentum and small center-of-mass (CM) momentum, where large and small is relative to the Fermi momentum of the nucleus. We refer to these pairs as short-range correlated (SRC) pairs [5–7]. In the missing momentum range of $300 - 600$ MeV/c, these pairs were found to dominate the high-momentum tails of the nuclear wave functions, with neutron-proton (np) pairs nearly 20 times more prevalent than proton-proton (pp) pairs, and by inference neutron-neutron (nn) pairs. This is due to the strong dominance of the NN-tensor interaction, at the probed sub-fermi distances [8–10].

The association of the small ^{12}C$(e,e'pp)$ / ^{12}C$(e,e'pn)$ ratio, at $(e,e'p)$ missing-momenta of $300 - 600$ MeV/c, with dominance of the NN-tensor force, leads naturally to the quest to increase missing momenta. This allows looking for pairs that are even closer to each other, at distances in which the nuclear force changes from being predominantly tensor to the essentially unexplored repulsive interaction. We report here on a simultaneous measurement of the ^{4}He$(e,e'p)$, ^{4}He$(e,e'pp)$ and ^{4}He$(e,e'pn)$ reactions at $(e,e'p)$ missing-momenta from 400 to 830 MeV/c. The observed changes in the isospin composition of the SRC pairs as a function of the missing momentum are presented, discussed, and compared to calculations.

The experiment was performed in Hall A of Jefferson Laboratory (JLab) using a 4 μA electron beam with energy of 4.454 GeV incident on a high pressure (13 atm) ^{4}He gas target at 20 K. The 20 cm long gas target had a density of 0.033 g/cm^3, and was contained in an aluminum cylinder with a 4 cm radius.

The two Hall A high resolution spectrometers (HRS) [11] were used to identify ^{4}He$(e,e'p)$ events. Scattered electrons were detected in the left HRS (L-HRS) at a central scattering angle of 20.3° and momentum of 3.602 GeV/c. This kinematic corresponds to the quasi-free knockout of a single proton with transferred three-momentum $|\vec{q}| \approx 1.64$ GeV/c, transferred energy $\omega \approx 0.86$ GeV, the negative four-momentum transfer squared $Q^2 = 2$ (GeV/c)^2, and $x_B = \frac{Q^2}{2m_p\omega} = 1.2$, where m_p is the proton mass. Knocked-out protons were detected using the right HRS (R-HRS) which was set at 3 different central angles and momenta: (33.5°, 1.38 GeV/c), (29°, 1.3 GeV/c), and (24.5°, 1.19 GeV/c). These kinematical settings correspond to $(e,e'p)$ central missing-momentum ($\vec{p}_{\rm miss} = \vec{p}_p - \vec{q}$) values of 500 MeV/$c$, 625 MeV/$c$, and 750 MeV/$c$, respectively, and covering a missing momentum range of $400 - 830$ MeV/c, with overlap between the three different settings. The angle between $\vec{q}$ and the recoil nucleon was $40 - 50$°.

For highly correlated pairs, the missing momentum of the $A(e,e'p)$ reaction is expected to be balanced almost entirely by a single recoiling nucleon. A large acceptance spectrometer (BigBite) followed by a neutron detector (HAND) with matching solid angles were used to detect such correlated recoiling protons or neutrons. The layout of the experimental setup is schematically presented in Fig. 1.

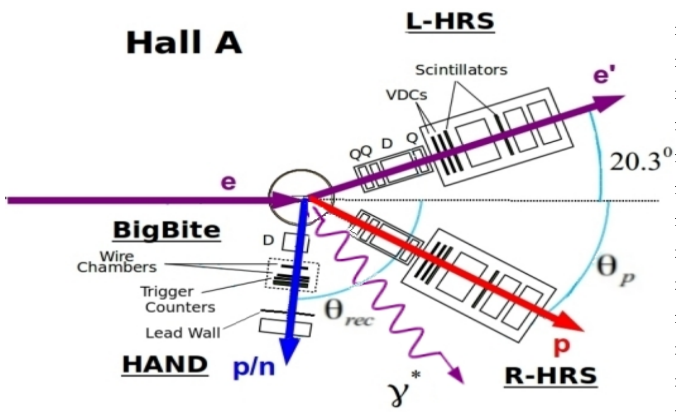

FIG. 1. A vector diagram of the layout of the experiment. The electron kinematics was fixed and three combinations of $\theta_p/\ P_p$ were used to cover the full missing momentum range. See text for details. The spectrometers are shown with their magnets (D-dipole, Q-quadropole) and their main detection systems, more details in Ref.[11].

The BigBite spectrometer [12] consists of a large acceptance, non-focusing dipole magnet followed by a detector package consisting of two planes of plastic scintillators (ΔE - E), referred to collectively as the trigger counters, and two wire chambers. The magnet was centered at an angle of 97°, for the 500 and 625 MeV/c measurements, and 92° for the 750 MeV/c measurement. The angular acceptance was about 96 msr and the detected momenta acceptance ranged from 0.25 GeV/c to 0.90 GeV/c.

The Hall A neutron detector (HAND) consists of several elements. A 2.4 cm thick lead shield (to block low-energy photons and most of the charged particles coming from the target), followed by 64 2-cm thick scintillators (to identify and veto charged particles), and 112 plastic scintillator bars arranged in six 10-cm thick layers covering an area of 1x3 m^2 (to detect the neutrons). The neutron detector array was placed six meters from the target, just behind BigBite, covering a similar solid angle as BigBite.

The experiment triggered on e-p coincidences between the HRS spectrometers, with BigBite and HAND detectors read out for every trigger. Thus, we could determine simultaneously the triple/double coincidence ratios: ^{4}He$(e,e'pp)/^4$He$(e,e'p)$, ^{4}He$(e,e'pn)/^4$He$(e,e'p)$ as well as the triple/triple coincidence ratio, ^{4}He$(e,e'pp)/^4$He$(e,e'pn)$.

The ^{4}He$(e,e'p)$ events were selected by placing a $\pm3\sigma$ cut around the coincidence timing peak which had a resolution of $\sigma = 0.6$ ns. The resulting event sample contained $1-9\%$ random events. The other cuts on the $(e,e'p)$ data were the nominal HRS phase-space cuts on momentum ($|\Delta p/p| \leq 0.045$), and angles ($\pm$60 mrad vertical, $\pm$30 mrad horizontal). To reduce the random-coincidence background, a cut on the target-reconstructed vertex from the two HRSs ensured that, for every event, both the electron and the proton emerged from the same place in the ^{4}He target. A cut on the two-dimensional distribution of the y-scaling variable [13] versus ω and a missing mass cut were applied to remove the contribution from $\Delta(1232)$ excitation [14] (see appendix). With all these cuts applied, a data set of ^{4}He$(e,e'p)$ events was generated, each with a measured missing momentum.

The recoiling protons were identified in BigBite using the measured energy loss in the ΔE - E scintillator detectors, the measured time-of-flight (TOF), and the momentum reconstructed using the trajectory in the magnetic field. The momentum resolution of BigBite, determined from elastic electron-proton scattering, was $\Delta p/p = 1.5\%$. The overall proton detection efficiency, as measured with e-p elastic scattering, was 73 $\pm$ 1%, primarily due to the gaps between scintillators and the tracking inefficiency of the wire chambers.

The pattern of hits in sequential layers of HAND was used to identify neutrons [15]. The momentum of the neutrons was determined using the measured TOF between the target and HAND. A time resolution of 1.5 ns allowed determination of the neutron momentum with an accuracy that varied from 2.5% (at 400 MeV/c) to 5% (at 830 MeV/c). The neutron detection efficiency was $40\pm1.4\%$ for $400-830$ MeV/c neutrons. This determination is based on the efficiency measured up to 450 MeV/c using the $d(e,e'pn)$ reaction, and extrapolation using a simulation that reproduces well the measured efficiency at lower momenta [16].

Figure 2 shows the distribution of the cosine of the angle between the missing momentum and the recoiling neutrons (γ). We also show the angular correlation for the random background as defined by a time window off the coincidence peak. The back-to-back peak of the real triple coincidence events is demonstrated clearly. The curve is a result of a simulation of the scattering of a moving pair having a center-of-mass (CM) momentum width of 100 MeV/c as discussed below. Similar back-to-back correlations were observed for the recoiling protons detected in BigBite. The timing peak shown in the insert of Fig. 2 is due to real triple coincidences and the flat background is due to random coincidences between the ^{4}He$(e,e'p)$ reaction and neutrons in HAND. The signal to background ratio at the three kinematics setups were $1:2-2.5$.

Figure 3 shows the missing mass and energy for the ^{4}He$(e,e'pp)$ reaction corresponding to a two-neutron residual system. Taking into account the binding energy of the two protons, the excitation energy and the CM kinetic energy of the residual two-neutron system is relatively low supporting the picture that they are essentially spectators in a reaction that breaks a pp-SRC pair. Similar missing-energy and -mass distributions were obtained for the ^{4}He$(e,e'pn)$ reaction but with inferior resolution

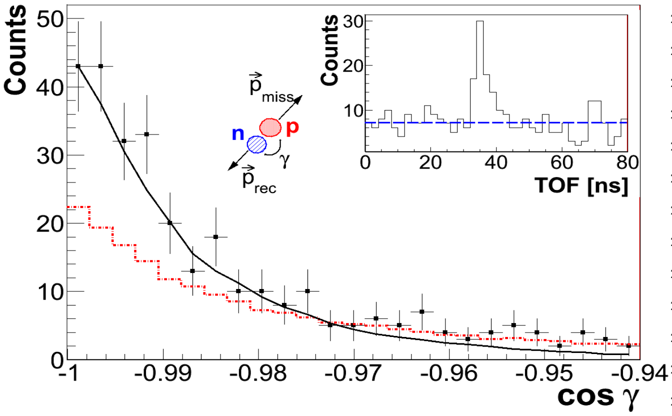

FIG. 2. The distribution of the cosine of the opening angle γ between the $\vec{p}_{\rm miss}$ and $\vec{p}_{\rm recoil}$ for the $p_{\rm miss} = 625$ and 750 MeV$/c$ kinematics combined. The histogram (dashed dotted, red online) shows the distribution of random events. The solid curve is a simulation of scattering off a moving pair with a CM momentum having a width of 100 MeV$/c$. The insert is the TOF spectrum for neutrons detected in HAND in coincidence with the ^{4}He$(e,e'p)$ reaction in the highest missing-momentum kinematics. The random background is shown as a dashed line.

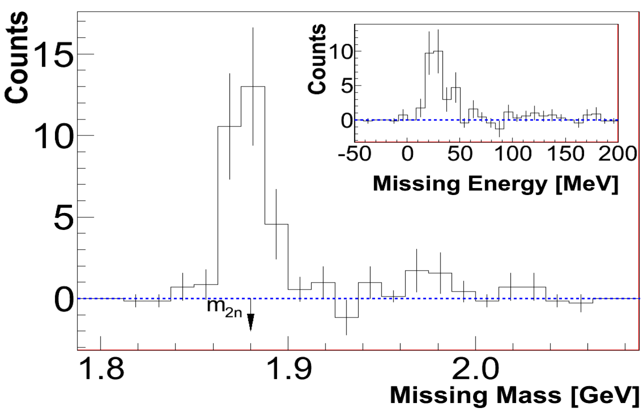

FIG. 3. The background subtracted missing-mass distribution for ^{4}He$(e,e'pp)$ events. The insert represents the background subtracted missing energy for the ^{4}He$(e,e'pp)$ events. Note that subtracting the binding energy of the two protons leaves the two neutrons residual system with a low excitation energy.

due to the lower momentum resolution for neutrons.

Software cuts were applied to both BigBite and HAND that limited their acceptances to be $\pm 14^\circ$ in the vertical direction, $\pm 4^\circ$ in the horizontal direction, and $300-900$ MeV$/c$ in momentum. We used a simulation based on the measurements to correct the yield of the ^{4}He$(e,e'pN)$ events for the finite acceptances of the recoiling protons and neutrons in Bigbite and HAND. Following Ref. [1], the simulations assume that an electron scatters off a moving SRC pair with a CM momentum relative to the $A-2$ spectator system described by a Gaussian distribution as in [17]. We assumed an isotropic 3-dimensional motion of the pair and varied the width of the Gaussian motion equally in each direction until the best agreement with the data was obtained. The nine measured distributions (three components in each of the three kinematic settings for np pairs) yield, within the uncertainties, the same width with a weighted average of 100 ± 20 MeV$/c$. This is in good agreement with the CM momentum distribution calculated in Ref. [10]. Figure 2 compares the simulated and the measured distributions of the opening angle between the knocked-out and recoiling nucleons. The fraction of events detected within the finite acceptance was used to correct the measured yield. The uncertainty in this correction was typically 15%, which dominates the systematic uncertainties of the ^{4}He$(e,e'pN)$ yield.

The measured $\frac{^4\text{He}(e,e'pN)}{^4\text{He}(e,e'p)}$ ratios are given by the number of events in the background-subtracted triple-coincidence TOF peak (as shown in the insert in Fig. 2) corrected for the finite acceptance and detection efficiency of the recoiling nucleons, divided by the number of random-subracted double coincidence ^{4}He$(e,e'p)$ events. These ratios, as a function of $p_{\rm miss}$ in the ^{4}He$(e,e'p)$ reaction, are displayed as full symbols in the two upper panels of Fig. 4. Because the electron can scatter from either proton of a pp pair (but only from the single proton of an np pair), we divided the ^{4}He$(e,e'pp)$ yield by two. Also displayed in Fig. 4, as empty symbols with dashed bars, similar ratios for ^{12}C obtained from previous electron scattering [1, 2] and proton scattering [4] measurements. In comparing the ^{12}C and ^{4}He data notice that there is a difference in the naive counting ratio of $\frac{NZ}{Z(Z-1)}$ between the two cases. The horizontal bars show the overlapping momentum acceptance ranges of the various kinematic settings. The vertical bars are the uncertainties, which are predominantly statistical.

Because we obtained the ^{4}He$(e,e'pp)$ and ^{4}He$(e,e'pn)$ data simultaneously and with the same solid angles and momentum acceptances, we could also directly determine the ratio of ^{4}He$(e,e'pp)$ to ^{4}He$(e,e'pn)$. In this ratio, many of the systematic factors needed to compare the triple-coincidence yields cancel out, and we need to correct only for the detector efficiencies. This ratio as a function of the missing momentum is displayed in the lower panel of Fig. 4 together with the previously measured ratio for ^{12}C [2].

To correct for final-state interactions (FSI), we calculated the attenuations of the leading and recoiling nucleons as well as the probability for single-charge-exchange (SCX) using the Glauber approximation [18]. To a good approximation the correction to the ratios due to the leading-proton attenuation is small. The attenuation of the recoiling nucleon decreases the measured triple/double coincidence ratios. Because the measured ^{4}He$(e,e'pn)$ rate is about an order of magnitude larger

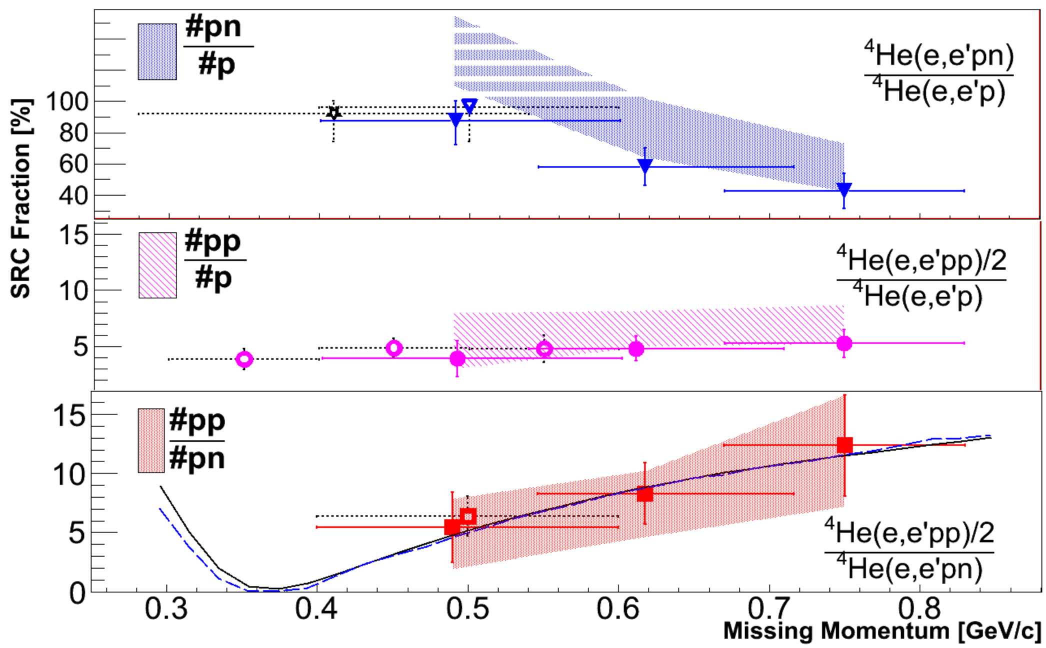

FIG. 4. Lower panel: The measured ratios ^{4}He$(e,e'pp)/$ ^{4}He$(e,e'pn)$ are shown as solid symbols as a function of the ^{4}He$(e,e'p)$ missing momentum. Each point is the result of a different spectrometers setting. The bands represent the data corrected for FSI to obtain the pair ratios, see text for details. Also shown are calculations using the momentum distribution of [10] for pairs with no CM momentum (dashed blue line) and with weighted-average CM momentum assuming arbitrary angles between it and the relative momentum in the pair (solid black line). The middle panel shows the measured ^{4}He$(e,e'pp)/$ ^{4}He$(e,e'p)$ and extracted $\#pp/\#p$ ratios. The upper panel shows the measured ^{4}He$(e,e'pn)/^4$He$(e,e'p)$ and extracted $\#pn/\#p$ ratios The unphysical region above 100% obtained due to statistical fluctuations is marked by white strips. Ratios for ^{12}C are shown as empty symbols with dashed bars. The empty star is the BNL result [4] for ^{12}C$(p,2pn)/^{12}$C$(p,2p)$. See text for a comment on the ^{12}C/ ^{4}He naive counting ratios.

than the ^{4}He$(e,e'pp)$ rate, ^{4}He$(e,e'pn)$ reactions followed by a single-charge exchange (and hence detected as ^{4}He$(e,e'pp)$) increase the ^{4}He$(e,e'pp)/^4$He$(e,e'pn)$ and the ^{4}He$(e,e'pp)/^4$He$(e,e'p)$ measured ratios.

The Glauber corrections ($T_{\rm L} = 0.75$ and $T_{\rm R} = 0.66 - 0.73$), where $T_{\rm L}$ and $T_{\rm R}$ the leading and recoil transparencies, were calculated by the Ghent group [18]. We assumed the uncertainties to be $\pm 20\%$ of these values. The probability for SCX ($P_{\rm SCX}$) was assumed to be $1.5 \pm 1.5\%$ based on the SCX total cross section of 1.1 ± 0.2 mb [19]. The pair fraction extracted from the measured ratios with the FSI calculated corrections are shown in Fig. 4 as bands (see appendix for details). The statistical and systematic uncertainties of the measurements and the calculated corrections were treated as independent and combined by simulation to create the width of the one standard deviation bands shown in Fig. 4.

The two-nucleon momentum distributions were calculated for the ground states of ^{4}He using variational Monte-Carlo wave functions derived from a realistic Hamiltonian with two- and three-nucleon potentials [10]. The number of pp-SRC pairs is much smaller than np-SRC pairs for values of the relative nucleon momentum $K_{rel} \approx 400$ MeV/c. This is because the correlations induced by the tensor force are strongly suppressed in the case of the pp pairs, which are mostly in a $^1S_0$ state [8–10, 20]. As the relative momenta increase, the tensor force is less dominant, the role played by the short-range repulsive force increases and with it the ratio of pp/np pairs. The solid (black) curve in Fig. 4 was obtained using the weighted average of the calculations with arbitrary angles between $\vec{K}_{rel}$ and $\vec{K}_{CM}$, the CM momentum or the pair. The dashed curve (blue) is the calculations with $K_{CM} = 0$ which is very little different from the average and agrees quantitatively with the Perugia group calculations [20]. To compare the calculations to the data in Fig. 4 we assumed that the virtual photon hits the leading proton and $p_{\rm miss} = K_{rel}$ (PWIA).

To summarize, measurements reported here facilitate the isospin decomposition of the $2N$-SRC in the high-momentum tail of the nucleon momentum distribution. The small, relatively constant measured ^{4}He$(e,e'pp)/^4$He$(e,e'p)$ ratio reflects a small contribution from pp-SRC pairs, most probably dominated by the repulsive short-range force. The large ^{4}He$(e,e'pn)/^4$He$(e,e'p)$ ratio clearly shows np-SRC dominance. The observed reduction in the fraction of measured 2N-SRC contribution to the total $(e,e'p)$ removal strength as a function of the missing momentum can be due to increasing FSI and/or the onset of 3N-SRC [5]. A definitive conclusion on the relative contribution of these effects requires a more detailed theoretical study.

The missing-momentum dependence of the ^{4}He$(e,e'pn)/^4$He$(e,e'p)$ ratio, and the ^{4}He$(e,e'pp)/^4$He$(e,e'pn)$ ratio, which agree well with the calculated ratio of *pp*-SRC / *np*-SRC pairs in the ground state, reflect the transition from tensor force dominance to the repulsive force domain as the nucleons momenta increase. Comprehensive calculations, which take into account the full reaction mechanism in a relativistic treatment, as well as additional data with better statistics will allow a more detailed determination of the role played by the elusive repulsive short-range nucleon-nucleon interaction.

We would like to acknowledge the contribution of the Hall A collaboration and technical staff. We thanks C. Colle, W. Cosyn and J. Ryckebusch for the Glauber Calculations. We want to also thank R.B. Wiringa, R. Schiavilla, S. Steven, and J. Carlson for some of the calculations presented in Ref [10] that were provided specifically for this paper. Useful discussions with J. Alster, C. Ciofi degli Atti, W. Cosyn, A. Gal, L. Frankfurt, J. Ryckebusch, M. Strikman, and M. Sargsian, are gratefully acknowledged. This work was supported by the Israel Science Foundation, the U.S. National Science Foundation, the U.S. Department of Energy grants DE-AC02-06CH11357, DE-FG02-94ER40818, and U.S. DOE Contract No. DE-AC05 84150, Modification No. M175, under which the Southeastern Universities Research Association, Inc. operates the Thomas Jefferson National Accelerator Facility.

Appendix

To extract the SRC pair ratios $\#pp/\#np$, $\#pp/\#p$, and $\#np/\#p$) from the measured cross sections ratios ($R = \frac{^4\mathrm{He}(e,e'pp)}{^4\mathrm{He}(e,e'pn)}$, $R1 = \frac{^4\mathrm{He}(e,e'pn)}{^4\mathrm{He}(e,e'p)}$, $R2 = \frac{^4\mathrm{He}(e,e'pp)}{^4\mathrm{He}(e,e'p)}$) we assumed factorization and used the equations A.1-A.3 listed below:

$$\frac{\#pp}{\#np} = \frac{T_L \cdot R - P_{\mathrm{SCX}} \cdot \frac{\sigma_{en}}{\sigma_{ep}}}{2 \cdot T_L - 2 \cdot P_{\mathrm{SCX}} \cdot \frac{\sigma_{en}}{\sigma_{ep}} \cdot R} \tag{A.1}$$

$$\frac{\#pp}{\#p} = \frac{R_1 \cdot \frac{\sigma_{en}}{\sigma_{ep}} \cdot \frac{P_{\mathrm{SCX}}}{T_L} \cdot T_R - R_2 \cdot T_R}{2 \cdot (\frac{\sigma_{en}}{\sigma_{ep}} \cdot \frac{P_{\mathrm{SCX}}}{T_L} \cdot T_R)^2 - 2 \cdot T_R^2} \tag{A.2}$$

$$\frac{\#np}{\#p} = \frac{R_2 - 2 \cdot \frac{\#pp}{\#p} \cdot T_R}{\frac{\sigma_{en}}{\sigma_{ep}} \cdot \frac{P_{\mathrm{SCX}}}{T_L} \cdot T_R} \tag{A.3}$$

where σ_{ep} (σ_{en}) is the cross section for electron scattering off the proton (neutron) [21].

The expression for missing mass is:

$$M_{miss} = \sqrt{(\omega + M_A - E_f - E_{\mathrm{rec}})^2 - (\vec{q} - \vec{p}_f - \vec{p}_{\mathrm{rec}})^2} \tag{A.4}$$

M_A is the mass of ^{4}He and the mass of the deuteron when applying the $\Delta(1232)$ cut. E_f and p_f (E_{rec} and p_{rec}) are the energy and momentum of the knocked-out proton (recoil nucleon). The missing energy is given by:

$$E_{miss} = \omega - T_p - T_{rec} - T_B \tag{A.5}$$

where T_p, T_{rec}, and T_B are the kinetic energy of the knocked-out proton, recoil partner and remaining $A-2$ system, respectively.

---

* deceased

[1] R. Shneor *et al.*, Phys. Rev. Lett. **99**, 072501 (2007).
[2] R. Subedi *et al.*, Science **320**, 1426 (2008).
[3] A. Tang *et al.*, Phys. Rev. Lett. **90**, 042301 (2003).
[4] E. Piasetzky*et al.*, Phys. Rev. Lett. **97**, 162504 (2006).
[5] L.L. Frankfurt and M.I. Strikman, Phys. Rep. **76**, 215 (1981).
[6] L.L. Frankfurt and M.I. Strikman, Phys. Rep. **160**, 235 (1988).
[7] J. Arrington, D. Higinbotham, G. Rosner, and M. Sargsian, Prog. Part. Nucl. Phys. **67**, 898 (2012).
[8] R. Schiavilla, R. B. Wiringa, S. C. Pieper, J. Carlson, Phys. Rev. Lett. **98**, 132501 (2007).
[9] R. B. Wiringa *et al.*, Phys. Rev. **C78**, 021001 (2008).
[10] R. B. Wiringa, R. Schiavilla, S. Steven, C. Pieper, and J. Carlson, http://arxiv.org/abs/arXiv:1309.3794
[11] J. Alcorn *et al.*, Nucl. Instrum. Meth. In Physics Research **A 522** (2004) 294.
[12] M. Mihovilovič *et al.*, Nucl. Instrum. Meth. **A 686**, 20 (2012).
[13] D.B. Day *et al.*, Phys. Rev. Lett. **59**, 427 (1987).
[14] P. Monaghan, Ph.D. Thesis, MIT (2008).
[15] R. Subedi, Ph.D. Thesis, Kent State University (2007).
[16] R. A. Cecil, B. D. Anderson and R. Madey, Nucl. Instr. and Meth **161**, 439 (1979).
[17] C. Ciofi degli and S. Simula, Phys. Rev. **C53**, 1689 (1996).
[18] J. Ryckebusch *et al.*, Nucl. Phys. **A728**, 226 (2003); W. Cosyn *et al.*, Phys. Rev. **C77**, 034602 (2008), and W. Cosyn and J. Ryckebusch, private communication.
[19] J. L. Friedes, H. Palevsky, R. L. Stearns , and R. J. Sutter, Phys. Rev. Lett. **15**, 38 (1965).
[20] M. Alvioli *et al.*, Phys. Rev. **C85**, 021001(R) (2012), and C. Ciofi degli Atti, H. Morita, private communication.
[21] S. Rock *et al.*, Phys. Rev. Lett. **49**, 11391142 (1982).